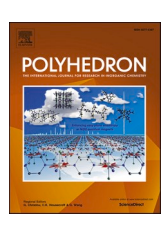


Contents lists available at ScienceDirect

# Polyhedron

journal homepage: www.elsevier.com/locate/poly



# Understanding the role of oxygen vacancies in SrTiO<sub>3</sub>/LaAlO<sub>3</sub> interfaces from first principles study

Ali H. Reshak

Physics department, College of Science, University of Basrah, Basrah 61004, Iraq

#### ARTICLE INFO

Keywords: Interface N-type 6.5STO/1.5LAO interfaces Oxygen vacancies

#### ABSTRACT

We have investigated the influence of oxygen vacancies on the electronic structure of 6.5STO/1.5LAO n-type interfaces. An 6.5STO/1.5LAO n-type interface along the (001) direction has been built. Then one oxygen atom has been removed to investigate the influence of an oxygen vacancy on the resulting properties. The original structure is designated as I and the one with O-vacancy as II. On the basis of that, a theoretical model originating from the designed O-vacancies was proposed to investigate the influence of the O-vacancy on the band structure and the associated properties. It was found that the O-vacancy leads to an increase in the effective masses and the density of states at the Fermi level (E<sub>F</sub>). Moreover, the O-vacancy leads to an increase in the valence electrons  $(Ve^-)$ . By increasing the  $Ve^-$  number, additional electrons  $(e^-)$  are added to the d-band at  $E_F$ . This leads to an increase of the carrier concentration. The calculated electronic charge density distribution is used to explore the influence of the O-vacancy on the bonding nature, charge transfer and electronic charge distribution. The Ovacancy adds two extra  $e^-$  to the interface to preserve charge neutrality. Adding 1e/unit cell or 0.5e/unit cell to the interface is enough to maintain overall neutrality. Moreover, the conductivity can be achieved only when The LaAlO<sub>3</sub>/SrTiO<sub>3</sub> interface is along the 001 crystallographic direction. The electrons at the interface between LAO/ STO are free to move parallel to the interface (xy plane), but are confined in the z direction (001) and thus can be thought of a two dimensional sheet of electrons sandwiched between two insulators. Interesting phenomena can result from this confinement of electrons in two dimensions due to the quantization of the electrons energy levels in the z-direction.

#### 1. Introduction

The interface between LaAlO<sub>3</sub> (LAO) and SrTiO<sub>3</sub> (STO) exhibits several interesting physical phenomena, such as quasi-2D electron transport with high electron mobility [1], 2D superconductivity at low temperatures [2], and electric field-tuned metal insulator and superconductor insulator phase transitions [3]. One of the notable examples is the interface between two band insulators with the perovskite ABO<sub>3</sub> structure, LaAlO<sub>3</sub> (LAO), and SrTiO<sub>3</sub> (STO) [4]. The n-type interface, in which the LAO layer is grown on top of TiO<sub>2</sub>-terminated STO, has highly mobile carriers, while the p-type interface, in which the LAO layer is grown on top of SrO-terminated STO, is totally insulating [1]. With the advance of techniques to control thin film growth on the atomic scale, the study of epitaxial oxide heterostructures is a rapidly developing area of materials science [5–10]. Due to the capability to fabricate a well-defined, single-terminated surface [6], oxide interfaces that are nearly atomically sharp can now be produced. In many cases, the properties of

these interfaces turn out to be much richer than those of their bulk constituents [7].

Not only are these new interface phases of fundamental physical interest, they are also promising candidates for novel devices and technology. Despite extensive efforts in both theory [8] and experiment [9], the origins of these interface properties are not yet completely understood. In part, this is due to the fact that more than one mechanism may play a role in determining the interesting behaviors. Also, which mechanism dominates the behavior in a given sample appears to be sensitive to the conditions under which the sample is grown and/or how it is processed prior to the experimental measurements [10]. As a result, direct comparison between experiments can be complicated. Nevertheless, progress is being made towards understanding the basis of the novel interface phenomena, in particular, the origin of the conductivity. To date, three mechanisms have been proposed to account for the emergence of conductivity at the SrTiO<sub>3</sub>/LaAlO<sub>3</sub> interface. The first mechanism is an intrinsic electronic reconstruction due to the polar

E-mail address: maalidph@yahoo.co.uk.

<sup>\*</sup> Corresponding author.

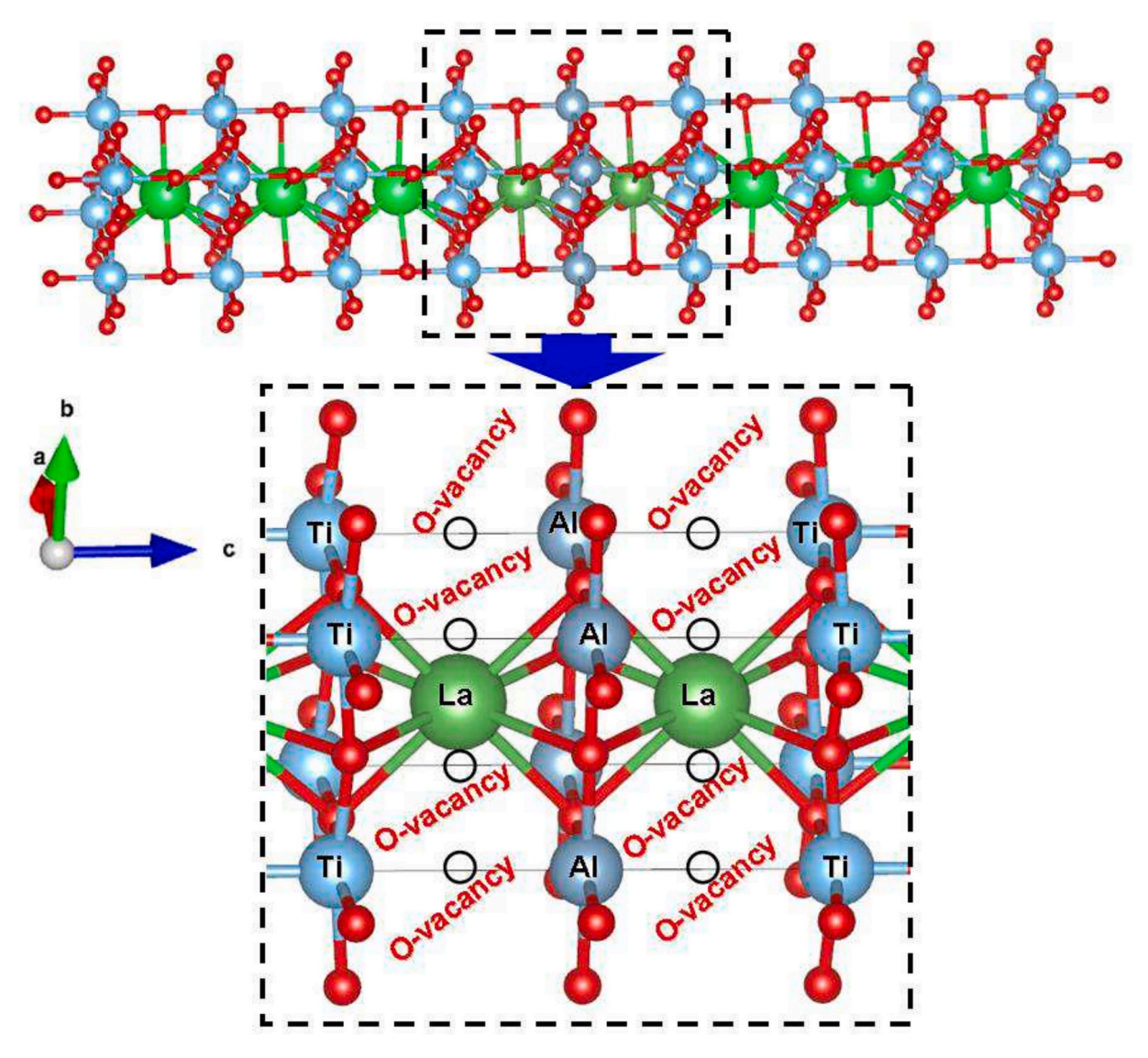
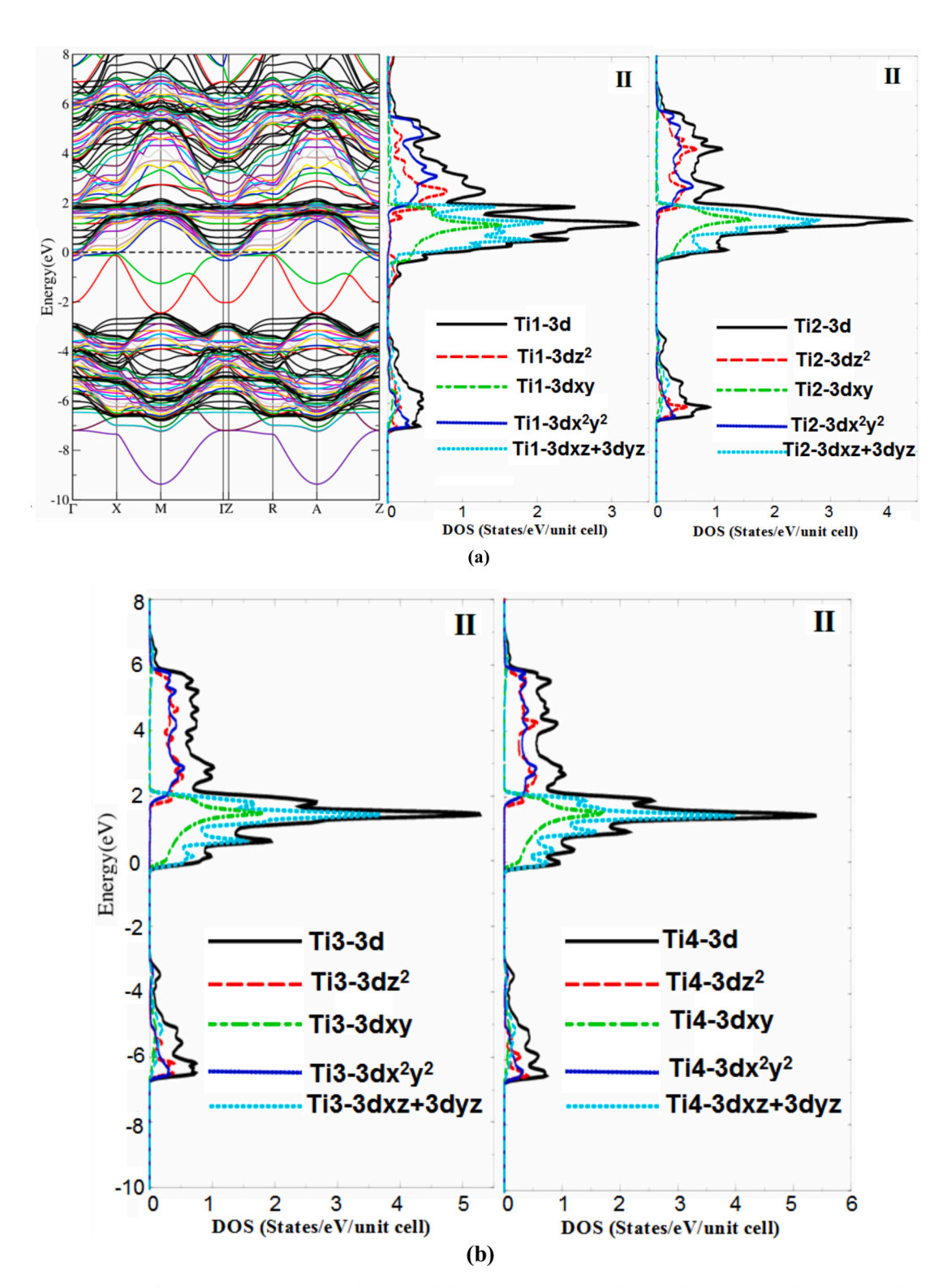


Fig. 1. Depiction of the type of symmetric structure, with two identical interfaces; it is assumed that a perfect STO layer (with TiO<sub>2</sub>-LaO planes at the interface) can be deposited on top of the LaO. A symmetric model interface was employed without the vacuum layer. The supercell has two symmetric n-type interfaces and there is no potential buildup due to symmetry. The two symmetric n-type interface along the (001) direction was built. Then one oxygen atom has been removed to investigate the influence of oxygen vacancy on the resulting properties. Consequently, a theoretical model originating from the designed oxygen vacancies was proposed in order to seek the influence of the oxygen vacancy on the band structure and the associated properties. The original compound was designated as I and the compound with oxygen vacancy as II. It can be seen that the eight oxygen atoms on both sides of the interface which are connected to Ti and Al atoms (Ti-O-Al) are absent in II.

discontinuity at the interface [11]. The driving force behind this mechanism can be understood in perovskite oxides that have a generic ABO<sub>3</sub> structure, where A and B are metal cations. As a consequence of this charge transfer, the interface becomes doped, leading to the observed conductivity. The second mechanism is based on oxygen vacancies [12,13] in the STO, which lead to the conductivity at the SrTiO<sub>3</sub>/ LaAlO<sub>3</sub> interface. Oxygen vacancies are also proposed [3] to account for the observed insulating-to-metallic transition, via a mechanism involving the creation and annihilation of oxygen vacancies on the LAO surface. The oxygen vacancy adds two extra electrons to the interface to preserve charge neutrality. Adding an 1e/unit cell or 0.5e/unit cell to the interface is enough to maintain overall neutrality. Undoubtedly, oxygen vacancies play an important role in the electronic properties of

the n-type SrTiO3/LaAlO3 interface [14]. A third possible mechanism, based on the observed intermixing of cations across the  $SrTiO_3/LaAlO_3$  interface, has also been suggested [15].

Several heterostructures have been studied in the literature; Chori et al. [16] presented the structural, optical, and electrical properties of La-doped SrTiO $_3$  epitaxial thin films. Kim et al. [16,17] investigated the structural, electronic, and magnetic properties of SrIrO $_3$ /SrTiO $_3$  using the first-principle calculations. Hotta et al. [18] investigated the transport properties of LaVO $_3$ /SrTiO $_3$ . Kalisky et al. [19] reported that the locally enhanced conductivity is due to the tetragonal domain structure in LaAlO $_3$ /SrTiO $_3$  heterointerfaces. Erlich et al. [20] confirm the explanation of the current channels and striped domains observed in the study of Kalisky et al. Bjaalie et al. [21] have used the hybrid DFT



**Fig. 2.** (a, b) Calculated electronic band structure of II along with the partial density of states of Ti1-3d<sub>xy</sub>, Ti2-3d<sub>xy</sub>, Ti3-3d<sub>xy</sub>, and Ti4-3d<sub>xy</sub>. Ti-3d orbits split into two parts: the  $t_{2g}$  ( $d_{xy}$ ,  $d_{xz}$ ,  $d_{yz}$ ) and  $e_g$  ( $d_{z2}$ ,  $d_{x2-y2}$ ) states; (c) The O-2p orbit split into  $p_\pi$  and  $p_s$  states.

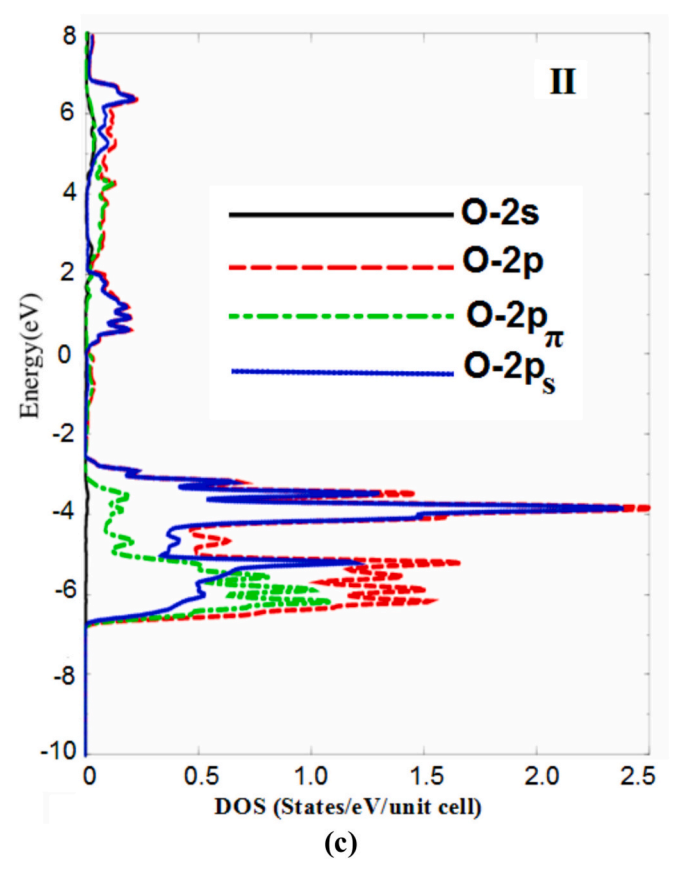


Fig. 2. (continued).

Table 1 The calculated density of states at  $E_F$ ,  $N(E_F)$  in (state/eV/unit cell) and the bare electronic specific heat coefficient ( $\gamma$ ) in mJ/(mol cell  $K^2$ ) for II in comparison to that of I.

	п		I	
	N(E <sub>F</sub> )	γ	N(E <sub>F</sub> )	γ
La	1.54	0.27	0.76	0.13
Sr	0.21	0.04	0.15	0.03
Ti1-d <sub>xv</sub>	4.39	0.76	4.33	0.75
Ti2-d <sub>xv</sub>	3.77	0.65	3.56	0.65
Ti3-d <sub>xy</sub>	3.38	0.59	2.90	0.50
Ti4-d <sub>xy</sub>	2.77	0.48	1.77	0.31
Al	0.12	0.02	0.0	0.0
0	0.22	0.04	0.12	0.02

Table 2 The calculated electron effective mass around  $\Gamma$  point of BZ for II in comparison to that of I.

	п	I
$m_e^*(\text{Ti1-d}_{xy})$	0.748 m <sub>e</sub>	0.7298 m <sub>e</sub>
$m_e^*$ (Ti2-d <sub>xy</sub> )	$0.6733 \ m_e$	$0.6514 \ m_e$
$m_e^*$ (Ti3-d <sub>xy</sub> )	$0.567 \ m_e$	$0.520 \; m_e$
$m_e^*$ (Ti4-d <sub>xy</sub> )	$0.555 \ m_e$	$0.485 \ m_e$

calculations to determine the band alignments of a number of complex oxides; considering materials with different types of conduction-band character, polar or nonpolar character and band insulators as well as Mott insulators were utilized. Drera et al. [22] have investigated the origin of electronic states at the basis of the 2DEG found in conducting LaAlO<sub>3</sub>/SrTiO<sub>3</sub> interfaces (5 u.c. LaAlO<sub>3</sub>) by resonant photoemission

experiments at the Ti  $L_{2,3}$  and La  $M_{4,5}$  edges. Salvinelli et al. [23] reported that the layer-resolved cation occupancy for different conducting and insulating interfaces of LaAlO<sub>3</sub> (LAO) thin films on SrTiO<sub>3</sub> (STO) has been determined by angle-resolved X-ray photoelectron spectroscopy. Das et al. [24] presented a study of  $\delta$  doping at the LaTiO<sub>3</sub>/SrTiO<sub>3</sub> interface with isostructural antiferromagnetic perovskite LaCrO<sub>3</sub>, which dramatically alters the properties of the two-dimensional electron gas at the interface. Furthermore, several workers [25–31] investigated the LaAlO<sub>3</sub>/SrTiO<sub>3</sub> interfaces.

To the best of our knowledge, most investigations on the electronic properties of the SrTiO<sub>3</sub>/LaAlO<sub>3</sub> interface have been done either experimentally or theoretically [11,12,24-44]. Some studies report the electronic properties of two symmetric n-type 6.5STO/1.5LAO interfaces [45-50], and some others [51,52] report the origin of the interface magnetism in BiMnO<sub>3</sub>/SrTiO<sub>3</sub> and magnetic and superconducting phases at the LaAlO<sub>3</sub>/SrTiO<sub>3</sub> interface. Recently, it has been found that the LaAlO3 (LAO) and SrTiO3 (STO) interface shows numerous promising applications [1–4]. The emergence of conductivity at the SrTiO<sub>3</sub>/LaAlO<sub>3</sub> interface could be attributed to the intrinsic electronic reconstruction due to the polar discontinuity at the interface [11]. Therefore, as a natural extension to our previous work [53,54], a step forward is necessary to understand the influence of the O-vacancies on the electronic charge density distribution and the electronic charge transfer at the interface of 6.5STO/1.5LAO because the O-vacancies at the LaAlO<sub>3</sub>/SrTiO<sub>3</sub> interface shows numerous promising applications for instance the LaAlO3/SrTiO3 show cathode luminescence, the development of next-generation electronic devices, a recent review by Kornblum focuses on detailing recent developments in field-effect devices based on conducting oxide interfaces [13,55-61]. We have performed comprehensive theoretical investigations based on the all-electron full-potential (FP-LAPW+lo) method within two kinds of exchange correlations namely; generalized gradient approximation (PBE-GGA) [62] and the Engel-Vosko GGA (EV-GGA) formalism [63]. To ascertain the influence of the XC on the resulting properties, EV-GGA formalism is the most capable of reproducing the exchange potential at the expense of less agreement in the exchange energy, which yields a better band splitting. We would like to mention that most of the previous works on the SrTiO3/LaAlO3 interface employed DFT within the local density approximation (LDA) or the generalized gradient approximation (GGA). In order to better describe strong electronic interaction between localized Ti-3d electrons [64-67]. While we decided to use the EV-GGA because it produces better band splitting; In general, in calculating the self-consistent band structure within DFT, both LDA and GGA usually underestimate the energy gap and band splitting [68]. This is mainly due to the fact that they have simple forms that are not sufficiently flexible to accurately reproduce both the exchange-correlation energy and its charge derivative. Engel and Vosko [63] considered this shortcoming and constructed a new functional form of GGA that is able to better reproduce the exchange potential at the expense of less agreement in the exchange energy. This approach, called EV-GGA, yields better band splitting and some other properties that mainly depend on the accuracy of the exchange-correlation potential [68,69].

#### 2. Methodology

The calculations are performed based on a symmetric supercell, with one  $AlO_2$  layer in the middle and two LaO layers around it, as well as alternating layers of  $TiO_2$  with SrO on both sides, as shown in Fig. 1. Brillouin zone of the 40 atom supercell was sampled with a 8x8x1 k-point grid. In our calculations, the two symmetric n-type interface is along the (001) direction so that the z-axis is perpendicular to the interface. GGA method was used to relax the atomic positions in the supercell. We fixed the in-plane lattice constant (parallel to the interface) at the experimental value of STO a = 3.91 A $^0$ , while the length of the supercell in the direction normal to the interface (out-of-plane) was

taken to be 8a. Atomic positions have been relaxed for the supercell by minimizing the forces on the atoms. All atoms are allowed to relax in the z direction until the force on each one is smaller than 1mRy/a.u. The supercell has two symmetric n-type interfaces and there is no potential buildup due to symmetry. The two symmetric n-type interfaces along the (001) direction has been built. Then one oxygen atom (Fig. 1) has been removed to investigate the influence of an oxygen vacancy on the resulting properties. On the basis of that, a theoretical model originating from the designed O-vacancies was proposed to investigate the influence of the O-vacancy on the overall properties. The compound without O-vacancy is designated as I and the one with O-vacancy as II. Following Fig. 1, it can be seen that the eight O atoms on both sides of the interface which are connected to Ti and Al atoms (Ti-O-Al) in I were removed in II.

The geometrical relaxation of I and II was achieved within the Perdew-Burke-Ernzerhof generalized gradient approximation (PBE-GGA) [62] using the full-potential linear augmented plane wave (FPLAPW+lo) method as embodied in the Wien2k code [70]. The resulting relaxed geometry is used to calculate the electronic structure and hence the associated properties using the Engel-Vosko GGA (EVGGA) formalism [63]. The muffin-tin radius ( $R_{\rm MT}$ ) was chosen to be 2.5, 2.46, 1.83, 1.74 and 1.62 a.u. for La, Sr, Ti, Al, and O, respectively. The  $R_{\rm MT} \times K_{\rm max}$ parameter was taken to be 7.0 to determine the matrix size,  $R_{\rm MT}$  being the smallest radius of the muffin-tin sphere, while  $K_{\text{max is}}$  the maximum modulus for the reciprocal lattice vectors K. The valence wave functions inside the muffin-tin spheres were expanded up to  $l_{max} = 10$ , while the charge density was Fourier expanded up to  $G_{max} = 12 (a.u)^{-1}$ . Selfconsistency was obtained using 500  $\bar{k}$  points in the irreducible Brillouin zone (IBZ). The self-consistent calculations were converged, since the total energy of the system is stable within 0.00001 Ry. The calculations of the electronic band structures, density of states, electronic charge density and Fermi surface were performed within 3000  $\bar{k}$  points in the IBZ. The first-principles calculations are a powerful and useful tool

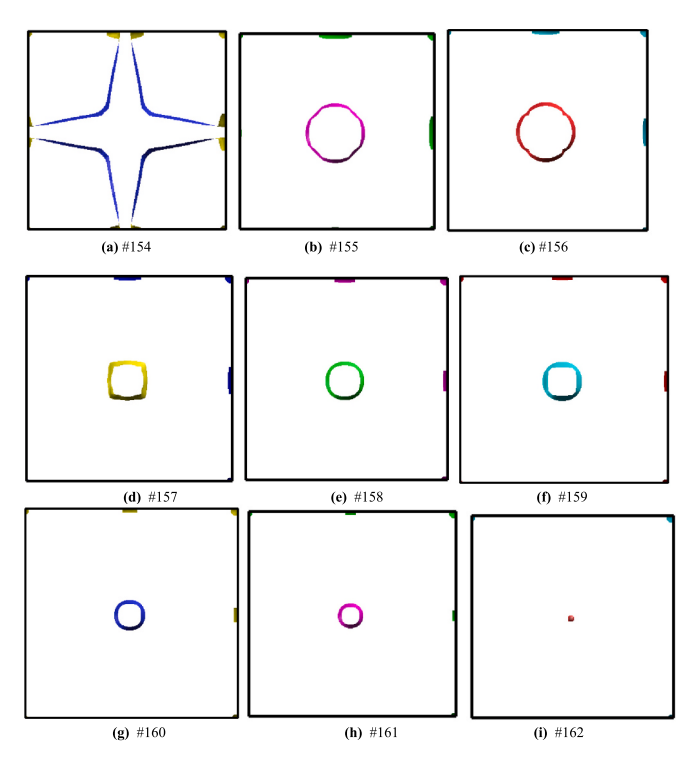


Fig. 3. (a-j) Calculated Fermi surface for I; (k) shows the bands which contribute to forming the Fermi surface of II in the first BZ. The left panel shows the Fermi surface along the high symmetry points  $\Gamma$ , X, Z, R, while the right panel shows the bands which form the Fermi surface around  $\Gamma$ -Z directions.

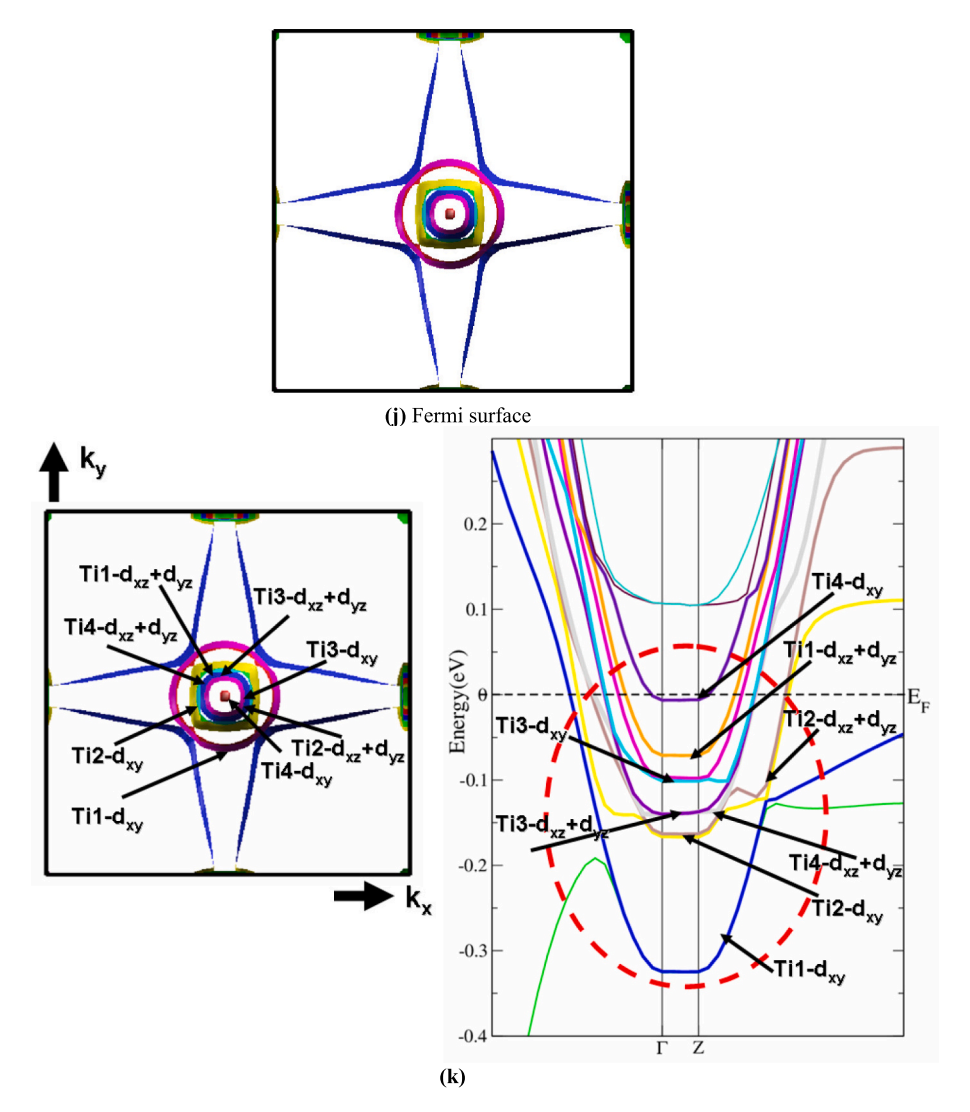


Fig. 3. (continued).

to predict the crystal structure and its properties related to the electron configuration of a material before its synthesis [71–75]. We would like to mention here that in our previous works [71–75] we have calculated several properties using FPLAPW method on several systems whose properties are known experimentally, in those previous calculations we found very good agreement with the experimental data. Thus, we believe that our calculations reported in this paper would produce very accurate and reliable results.

# 3. Results and discussion

The electronic band structure of compound II along the high symmetry directions is plotted side to side with the projected density of the states of Ti-3d, Ti-3d<sub>z2</sub>, Ti-3d<sub>xy</sub>, Ti-3d<sub>x2y2</sub> and Ti-3d<sub>xz</sub> + 3d<sub>yz</sub> states of the four Ti atoms in the layer neighboring the interface, as shown in Fig. 2 (a). It is interesting to mention that due to the O-vacancy, there are some energy bands appearing directly below  $E_F$  in the energy region between -0.5 and -3.0 eV of II; in comparison to I, this energy region is a forbidden gap (see Fig. 2(a) and the supplementary materials Fig. S1). This could be called the intermediate band (IB). The appearance of new bands may cause the appearance of new excitations. Recently, Ding et al. [76] reported that the position of such a local energy level is changed due to the variation of O-vacancy concentration. Moreover, the oxygen vacancy causes a push of the conduction bands towards  $E_F$ , resulting in the increasing the density of states at  $E_F$ , N( $E_F$ ) and the bare electronic

specific heat coefficient ( $\gamma$ ), in comparison to I (see Table 1). It is well known that the non-zero density of states at the  $E_F$  leads to unusual transport properties, and hence, large electrical conductivity ( $\sigma_{electrical}$ ). Similar behavior was observed in  $Co_2MnAl$  and  $Co_2MnSn$  compounds [77]. Therefore, the bands which cross  $E_F$  are responsible for the  $\sigma_{electrical}$  of the compound and those bands which do not cross  $E_F$  will contribute negligibly to the  $\sigma_{electrical}$  [78].

It has been also found that the O-vacancy leads to an increase in the valence electrons. By increasing the number of valence electrons ( $Ve^-$ ), additional electrons are added to the d-band at  $E_F$  [79]. This leads to an increase of the carrier concentration (n), and hence, the  $\sigma_{electrical}$ . Therefore, to achieve the highest  $\sigma_{electrical}$ , high mobility carriers are required. We have calculated the effective mass of electrons ( $m_e^*$ ) around  $\Gamma$  point of BZ for Ti1-3d<sub>xy</sub>, Ti2-3d<sub>xy</sub>, Ti3-3d<sub>xy</sub> and Ti4-3d<sub>xy</sub>, of I and II, as listed in Table 2. Following Table 2, it was found that the oxygen vacancy causes an increase in the  $m_e^*$  in concordance with previous work [80]. That is attributed to the fact that the electronic band structure shows that both I and II possess parabolic bands in the vicinity of  $E_F$  with different k-dispersions (Fig. 2a and supplementary materials Fig. S1).

According to the crystal field theory, due to the hybridization of Ti—O, the Ti-3d orbits split into two parts: the  $t_{2g}$  ( $d_{xy}$ ,  $d_{xz}$ ,  $d_{yz}$ ) and  $e_g$  ( $d_{z2}$ ,  $d_{x2-y2}$ ) states (see Figs. 2a,b and Fig. S2c supplementary materials). Geometrically,  $t_{2g}$  orbitals have lobes pointing between O-atoms, while  $e_g$  orbitals point towards O. The O-2p orbit splits into  $p_\pi$  and  $p_s$  states (see

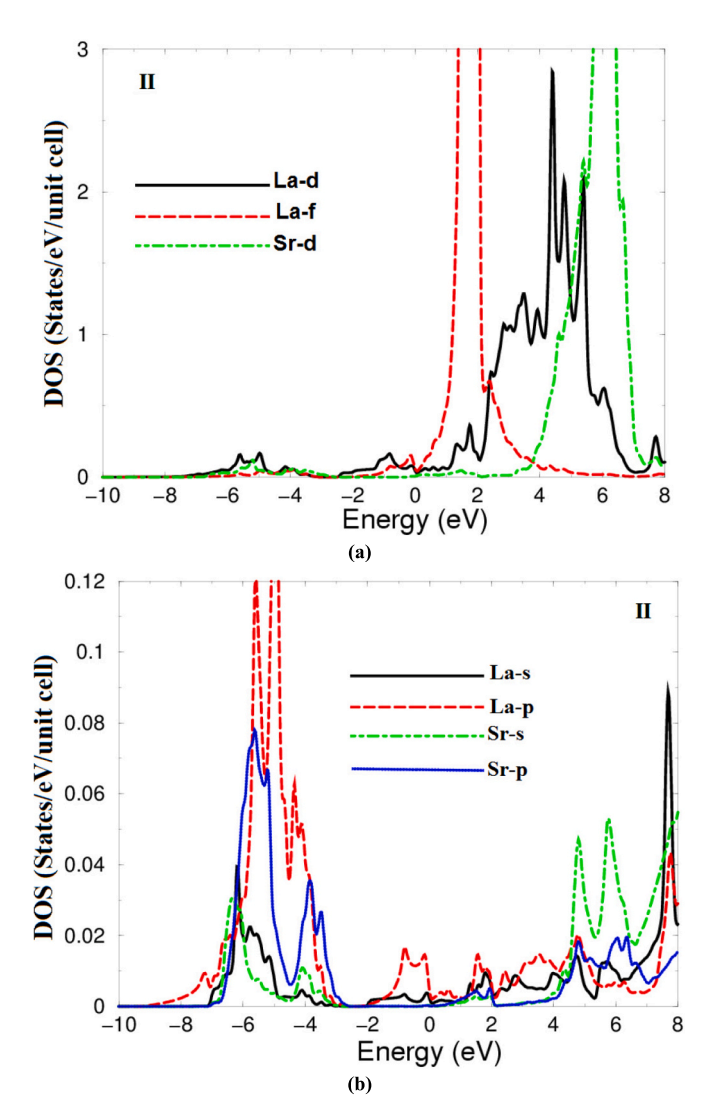


Fig. 4. (a-c) The angular momentum resolved projected density of states of La-6 s/5p/4d/4f, Sr-5 s/4p/3d, Al-3 s/3p and Ti-4 s/3p states for I.

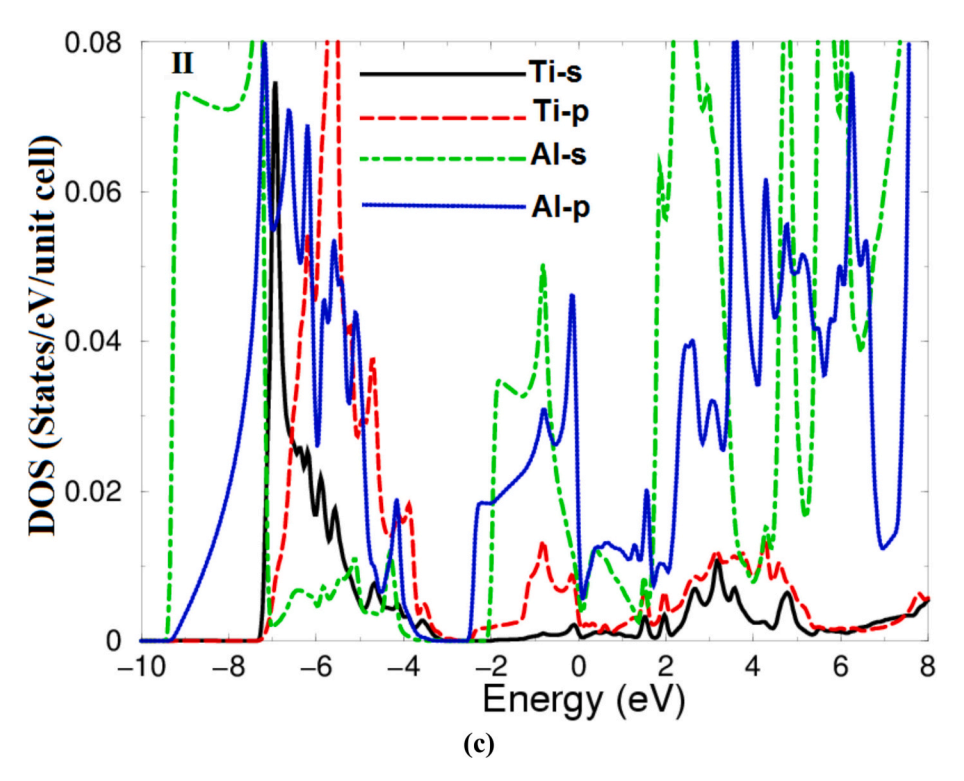


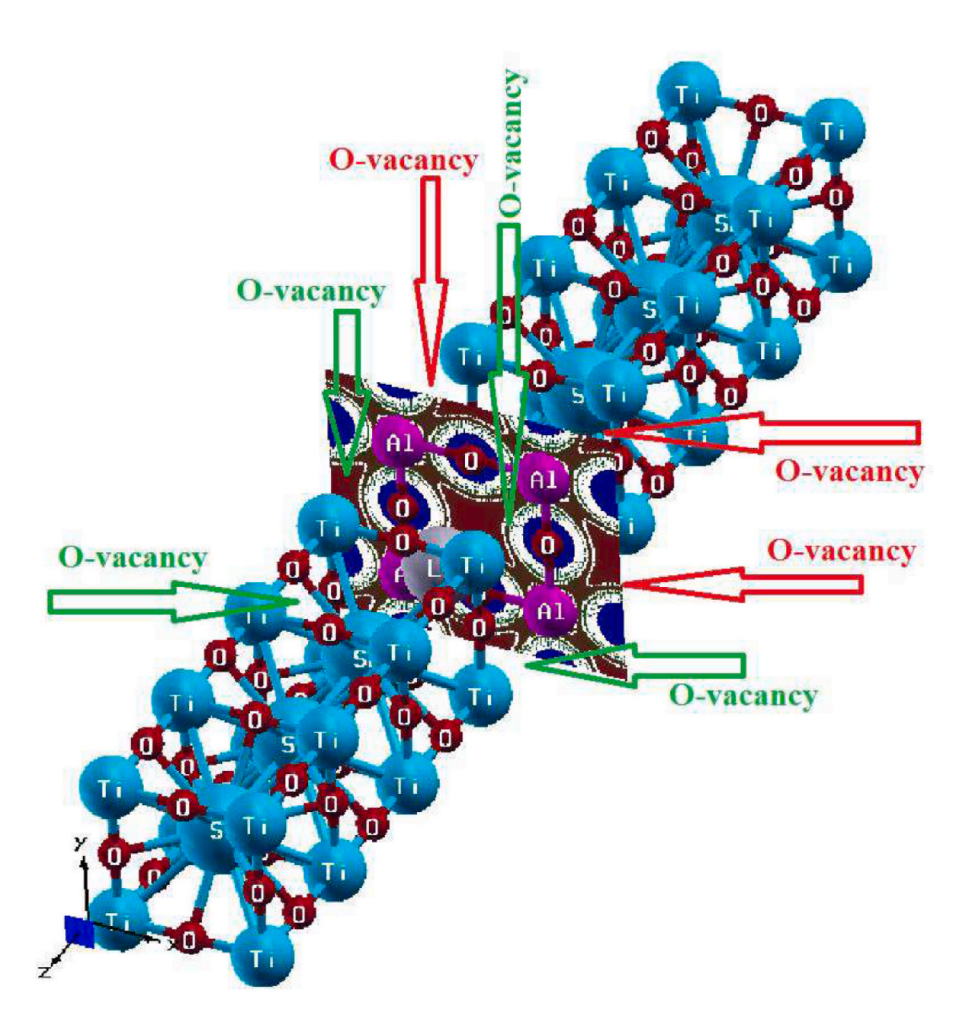
Fig. 4. (continued).

Fig. 2c). O-2p and  $t_{2g}$  ( $d_{xz}$ ,  $d_{yz}$ ) of Ti-3d devoted to the valence band (VB)  $(p_{\pi}$  devote to the top of the VB), while the conduction band (CB) was contributed by the  $d_{xy}$  and  $e_g$  of Ti-3d ( $d_{xy}$  devotes to the bottom of the CB) [81]. At the ionic limit, each Ti gives four electrons to two O atoms, resulting in the nominal charges of  $Ti^{4+}$  and  $O^{2-}$  [82]. Figs.2a-c illustrate the  $t_{2\rm g}$  ( $d_{
m xy}, d_{
m xz}, d_{
m yz}$ ) and  $e_{
m g}$  ( $d_{
m z2}, d_{
m x2-y2}$ ) states of Ti-3d and  $p_{
m \pi}$  and  $p_{
m s}$ states of O-2p. The O-vacancy causes an increase in the contribution of  $Ti1-3d_{xy}$ ,  $Ti2-3d_{xy}$ ,  $Ti3-3d_{xy}$  and  $Ti4-3d_{xy}$  around  $E_F$ , resulting in the strengthening of the density of states at E<sub>F</sub> (Table 1) and creates changes in their particular charge occupancies. This attributed due to the fact that the Ti-3d state is partially occupied reveals that there is mixed valency of Ti<sup>3+</sup> and Ti<sup>4+</sup>. It is clear that the Ti-3d<sub>xy</sub>, Ti-3d<sub>z2</sub>, Ti3-3d<sub>x2y2</sub> and  $Ti-3d_{xz}+d_{yz}$  cross  $E_F$  and form the Fermi surface (FS). The calculated FS of II is shown in Fig. 3(a-k). It is clear that the FS of II differs from that of I (supplementary materials Fig. S2 and Fig. 3k); at the FS of II there are high speed electrons at the center of BZ ( $\Gamma$  point) while these do not exist in I, which shows good agreement with previous work [46,50,83]; this implies less conductivity. It was noticed that at the FS there are white regions which represent the hole concentration, while the colored regions correspond to the presence of electrons [84]. Colors of the FS also give an idea about the speed of electrons ( $e^-$ ). The red color represents the highest speed, yellow, green and blue have intermediate speeds, whereas the violet color shows the lowest speed. The colors of the FS confirm that O-vacancy causes a reduction/increase in the speed of the  $e^-$  at the FS. Usually the thermoelectric properties are related to the  $e^-$  in the system, and these  $e^-$  are defined through the FS, which determines the  $\sigma_{electrical}$  [43]. Fig. 3k shows the bands which contribute to forming the FS of II in the first BZ. The left panel shows the FS along the high symmetry points  $\Gamma$ , X, Z, R, while the right panel shows the bands which form the FS around  $\Gamma$ -Z directions.

Furthermore, the angular momentum resolved projected density of states of La-6 s/5p/4d/4f, Sr-5 s/4p/3d, Al-3 s/3p and Ti-4 s/3p states are shown in Figs. 4(a-c) and O-2 s/2p states are shown in Fig. 2(c). Following these figures, the contribution of each orbital of La, Al, Sr, Ti and O atoms can be clearly seen. It was noticed that there are some orbitals which are contributing to form the FS in addition to Ti-3d<sub>xy</sub>, Ti-

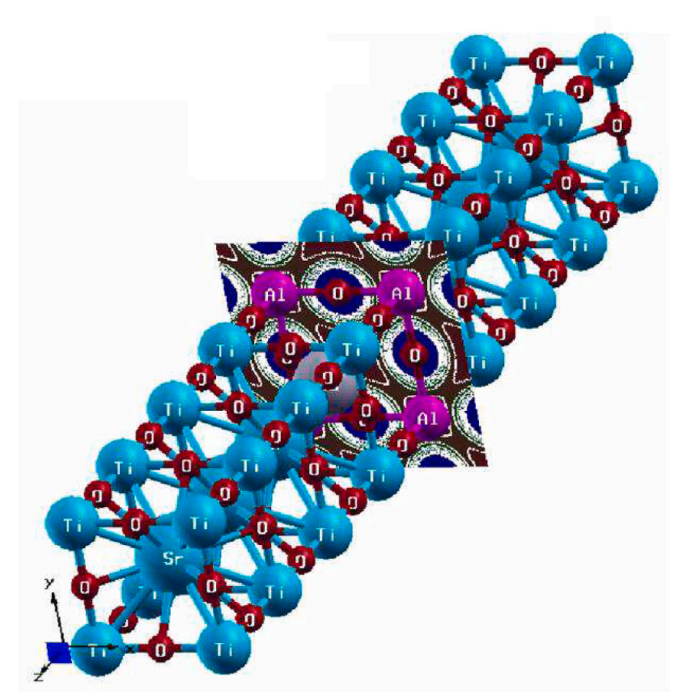
 $3d_{z2}$ ,  $Ti3-3d_{x2y2}$  and  $Ti-3d_{xz}+d_{yz}$ . A strong hybridization between La-6 s with Ti-4 s, Sr-5 s with Al-3 s, Ti-3p with O2-s/2p, Al-3p states, and Al-3p with Ti-4 s are observed. The hybridization may result in the formation of covalent bonding and the strengths of the covalency will depend on the degree of hybridization. To determine the influence of the O-vacancy on the bonds nature, the interactions between the atoms and the charge transfer, and the valence electronic charge density distribution at the interface are investigated. Fig. 5(a-f) shows the (001), (100) and (1/2 0 0) crystallographic planes. Fig. 5(a) shows that the (0 0 1) crystallographic plane of II in comparison to that of I (Fig. 5b). The area around the interface (Figs. 5c, d) has been enlarged to visualize the location of the oxygen vacancies. To gain detailed information about the influence of the oxygen vacancy on the interface (0 0 1), images of the interface in the (1 0 0) and (1/2 0 0) directions were collected (see Figs. 5e,f).

The crystallographic plane (1 0 0) of I in comparison with that of II clearly shows the influence of the oxygen vacancy on the bonding nature, charge transfer and electronic charge distribution. The O-vacancy adds two extra  $e^-$  to the interface to preserve charge neutrality. Adding a 1e/unit cell or 0.5e/unit cell to the interface is enough to maintain overall neutrality. Following these figures, we can obtain a clear map of the VB electronic charge density distribution of the two symmetric ntype 6.5STO/1.5LAO interfaces. The oxygen vacancy influences the oxygen atoms which are near Al; it is clear that both O and Al atoms are surrounded by a spherical charge; therefore, both O and Al exhibit an ionic nature. In contrast, the O atoms which are the nearest neighbors to Ti atoms exhibit partially covalent and mostly ionic bonding with Ti (see Fig. 5e) less than that in II. The weak covalent bonds between Ti and O atoms are due to the Pauling electronegativity differences between Ti (1.54) and O (3.44). It is clear that the (1/2 0 0) plane (Fig. 5f) exhibits all the atoms; each of the La and Sr atoms is surrounded by a spherical charge indicating the ionic bonding. Due to electronegativity differences between La (1.1), Al (1.61), Ti (1.54), Sr (0.95) and O (3.44), the charge is attracted towards O atoms which are surrounded by a blue spherical charge which indicated the maximum charge accumulation site in accordance with the charge density scale.



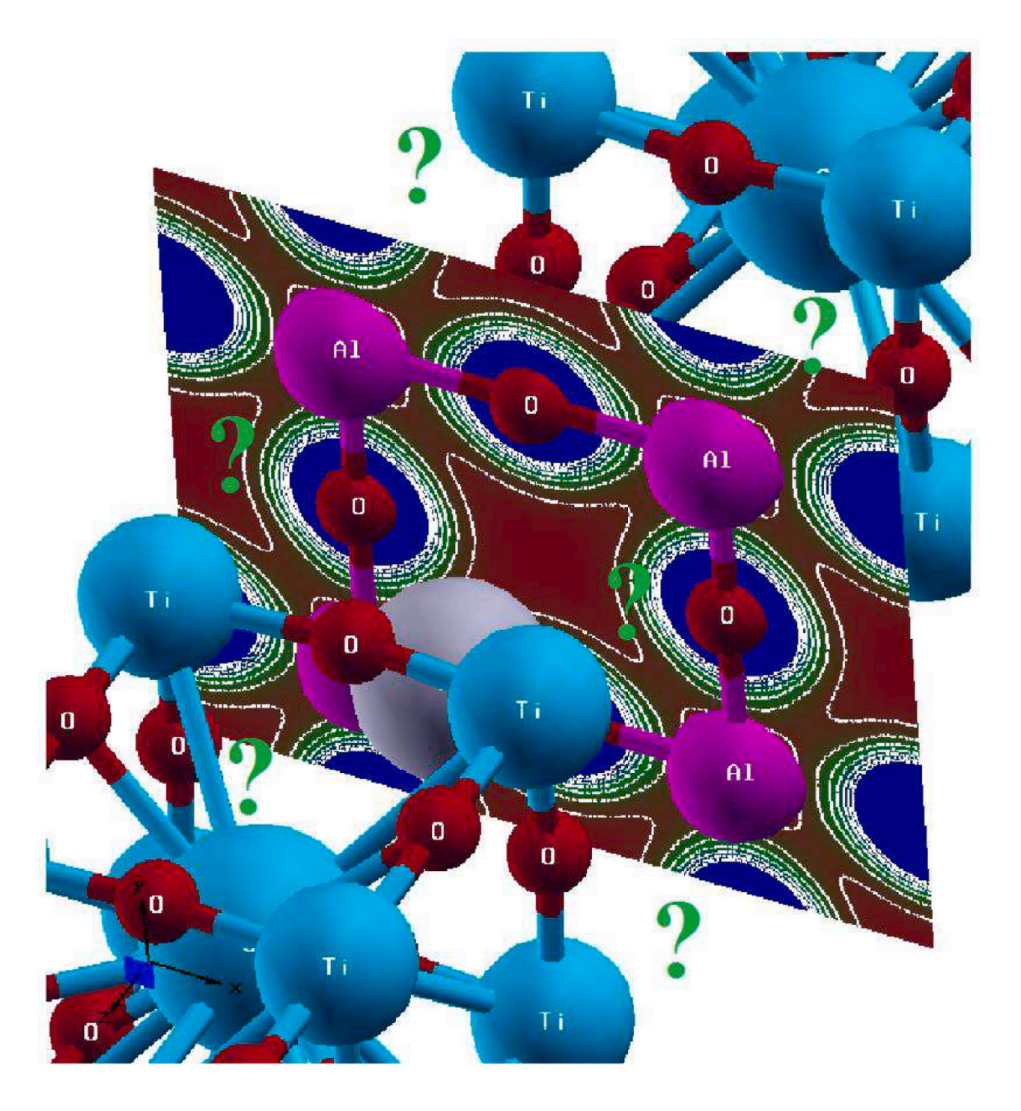
(a) (0 0 1) crystallographic plane of II. Which clearly that the eight oxygen atoms on both sides of the interface which are connected to Ti and Alatoms (Ti-O-Al) in I were removed in II.

Fig. 5. Calculated total valence charge density distribution of I for different crystallographic planes; (a)  $(0\ 0\ 1)$  crystallographic plane of II; (b)  $(0\ 0\ 1)$  crystallographic plane of I; (c)  $(0\ 0\ 1)$  crystallographic plane of II and I. These figures show that the eight oxygen atoms on both sides of the interface which are connected to Ti and Al atoms (Ti-O-Al) are absent in II.



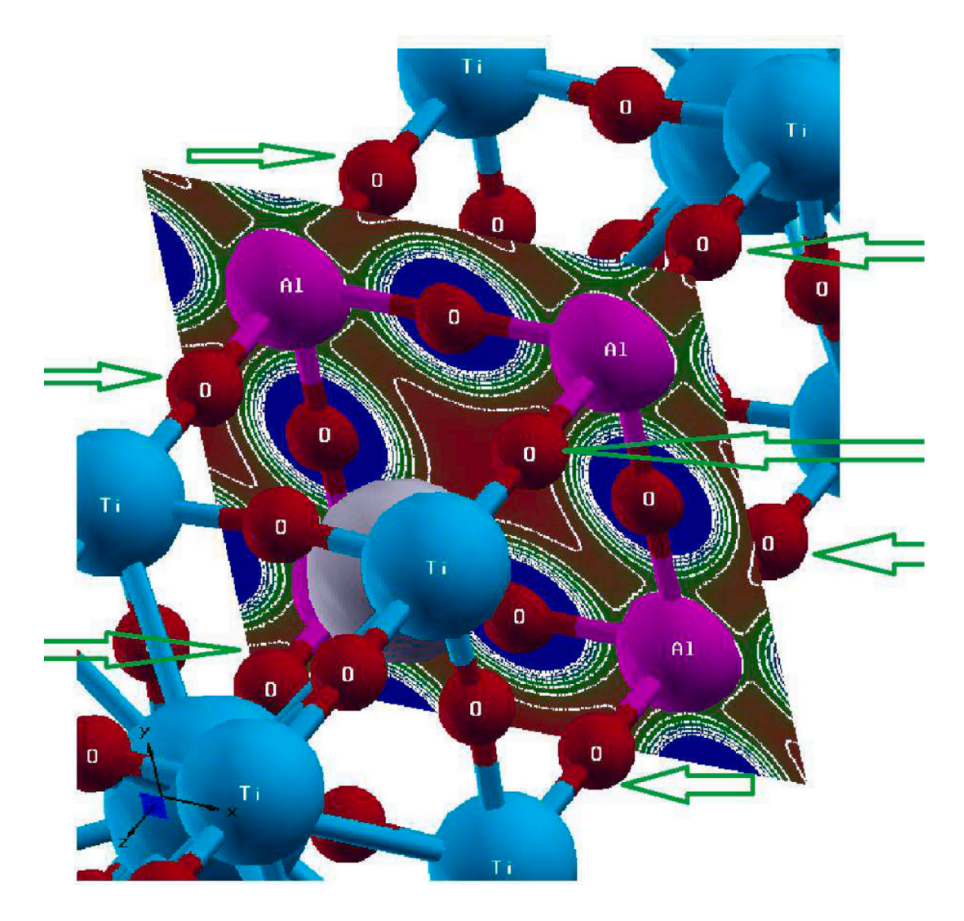
(b)  $(0\ 0\ 1)$  crystallographic plane of I.

Fig. 5. (continued).

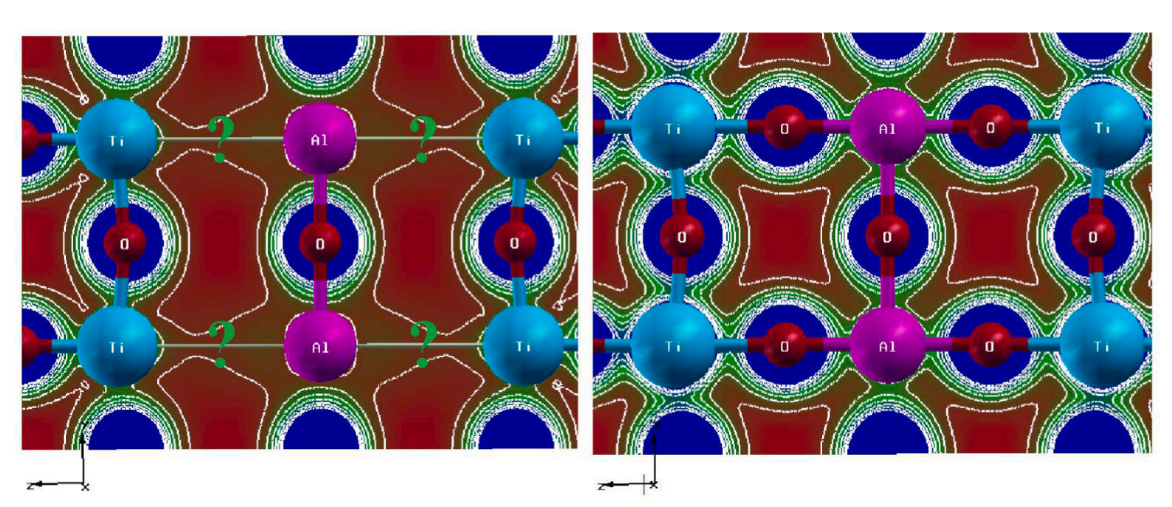


(c)  $(0\ 0\ 1)$  crystallographic plane of II. Which clearly that the eight oxygen atoms on both sides of the interface which are connected to Ti and Alatoms (Ti-O-Al) in I were removed in II.

Fig. 5. (continued).



(d) (0 0 1) crystallographic plane of I.



(e) (100) crystallographic plane of II and I. Which clearly that the eight oxygen atoms on both sides of the interface which are connected to Ti and Al atoms (Ti-O-Al) in I were removed in II.

Fig. 5. (continued).

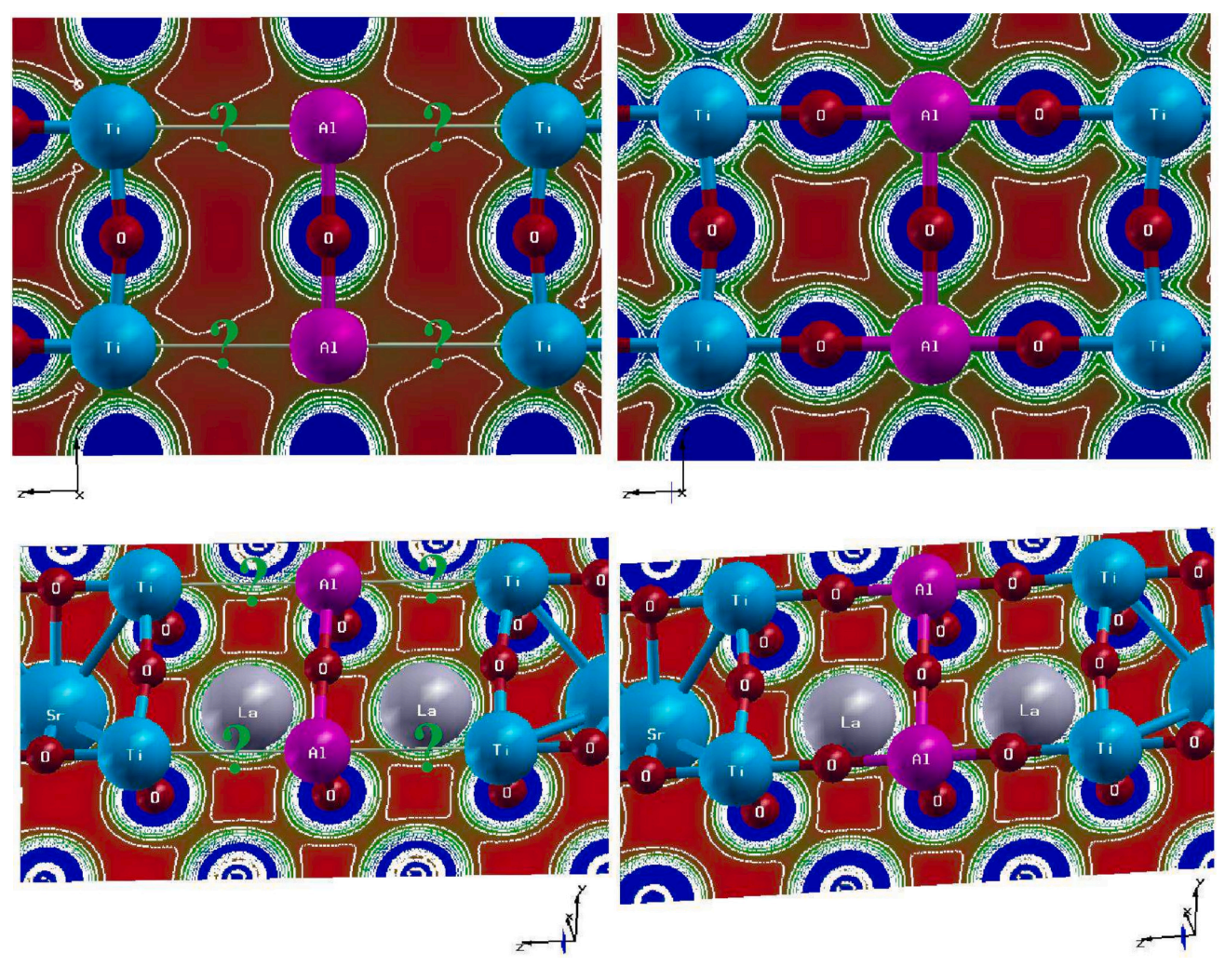


Fig. 5. (continued).

# 4. Conclusions

We have explored the influence of the oxygen vacancy on the electronic structure of two symmetric n-type 6.5STO/1.5LAO interfaces using the all-electron full-potential linearized augmented plane wave method plus the local orbitals (FP-LAPW+lo) approach. Due to the hybridization of Ti—O, the Ti-3d orbits split into two parts, the  $t_{2g}$  ( $d_{xy}$ ,  $d_{xz}$ ,  $d_{yz}$ ) and  $e_g$  ( $d_{z2}$ ,  $d_{x2-y2}$ ) states. Geometrically,  $t_{2g}$  orbitals have lobes pointing between O-atoms, while  $e_{\rm g}$  orbitals point towards O. The O-2p orbit split into  $p_{\pi}$  and  $p_{\rm s}$  states. O-2p and  $t_{\rm 2g}$   $(d_{\rm xz},\,d_{\rm yz})$  of Ti-3d devoted to the valence band ( $p_{\pi}$  devote to the top of the valence band), while the conduction band was contributed by the  $d_{xy}$  and  $e_g$  of Ti-3d ( $d_{xy}$  devotes to the bottom of the conduction band). In the ionic limit, each Ti gives four electrons to two oxygen atoms, resulting in the nominal charges of Ti<sup>4+</sup> and O<sup>2-</sup>. The attention was paid to the interaction between Ti and La at the interface. The strong interfacial hopping triggers a rise in the energy of the La  $d_{xy}$  state, and a lowering in the energy of the Ti  $d_{xy}$  state. Compared to the other Ti orbitals in the substrate, the Ti d orbitals at the two symmetric n-type interfaces are appropriate because they have more energy and are thus able to more effectively bind electrons to the interface. Therefore, a couple of bonding and antibonding states between the two cations are formed at the interface. The calculated valence band electronic charge density reveals that the charge is attracted towards oxygen atoms which are surrounded by uniform blue spheres which indicate the maximum charge accumulation. The oxygen vacancies play an important role in the electronic properties of the ntype SrTiO3/LaAlO3 interface. Moreover, the conductivity can be achieved only when The LaAlO3/SrTiO3 interface is along the 001 crystallographic direction. The electrons at the interface between LAO/STO are free to move parallel to the interface (xy plane), but are confined in the z direction (001) and thus can be thought of a two dimensional sheet of electrons sandwiched between two insulators. Interesting phenomena can result from this confinement of electrons in two dimensions due to the quantization of the electrons energy levels in the z-direction.

#### CRediT authorship contribution statement

Ali H. Reshak: Writing - review & editing, Writing - original draft.

# **Declaration of competing interest**

The authors declare that they have no known competing financial interests or personal relationships that could have appeared to influence the work reported in this paper.

### Appendix A. Supplementary data

Supplementary data to this article can be found online at https://doi.org/10.1016/j.poly.2025.117695.

#### Data availability

No data was used for the research described in the article.

#### References

- [1] A. Ohtomo, H.Y. Hwang, Nature 427 (2004) 423.
- [2] D.A. Dikin, M. Mehta, C.W. Bark, C.M. Folkman, C.B. Eom, V. Chandrasekhar, Phys. Rev. Lett. 107 (2011) 056802.
- [3] C. Cen, S. Thiel, G. Hammerl, C.W. Schneider, K.E. Andersen, C.S. Hellberg, J. Mannhart, J. Levy, Nat. Mater. 7 (2008) 298.
- [4] M. Huijben, A. Brinkman, G. Koster, G. Rijnders, H. Hilgenkamp, H.A. Blank, Adv. Mater. 21 (2009) 1665.
- [5] J.W. Reiner, F.J. Walker, C.H. Ahn, Science 323 (2009) 1018.
- [6] G. Koster, B.L. Kropman, G.J.H.M. Rijnders, D.H.A. Blank, H. Rogalla, Appl. Phys. Lett. 73 (1998) 2920.
- [7] M. Takizawa, Y. Hotta, T. Susaki, Y. Ishida, H. Wadati, Y. Takata, K. Horiba, M. Matsunami, S. Shin, M. Yabashi, K. Tamasaku, Y. Nishino, T. Ishikawa, A. Fujimori, H.Y. Hwang, Phys. Rev. Lett. 102 (2009) 236401.
- [8] (a) U. Schwingenschlogl, C. Schuster, Chem. Phys. Lett. 467 (2009) 354.(b)Chen, H.; Kolpak, A. M.; Ismail-Beigi, S., (arXiv:1008.3379 [cond-mat.mtrl-sci]), 19 Aug.
- [9] S. Thiel, C.W. Schneider, L. Fitting Kourkoutis, D.A. Muller, N. Reyren, A. D. Caviglia, S. Gariglio, J.-M. Triscone, J. Mannhart, J. Phys. Rev. Lett. 102 (2009) 046809.
- [10] J.N. Eckstein, Nat. Mater. 6 (2007) 473.
- [11] N. Nakagawa, H.Y. Hwang, D.A. Muller, Nat. Mater. 5 (2006) 204.
- [12] W. Siemons, G. Koster, H. Yamamoto, W.A. Harrison, G. Lucovsky, T.H. Geballe, D. H.A. Blank, M.R. Beasley, Phys. Rev. Lett. 98 (2007) 196802.
- [13] A. Kalabukhov, R. Gunnarsson, J. Borjesson, E. Olsson, T. Claeson, D. Winkler, Phys. Rev. B 75 (2007) 121404.
- [14] Karolina Janicka, Two dimensional electron gas at oxide interfaces, Theses, Dissertations, and Student Res.: Department of Phys. and Astronomy. Paper 18 (2011). http://digitalcommons.unl.edu/physicsdiss/18.
- [15] P.R. Willmott, S.A. Pauli, R. Herger, C.M. Schlepütz, D. Martoccia, B.D. Patterson, B. Delley, R. Clarke, D. Kumah, C. Cionca, Y. Yacoby, Phys. Rev. Lett. 99 (2007) 155502
- [16] M. Choi, A.B. Posadas, C.A. Rodriguez, A. O'Hara, H. Seinige, A.J. Kellock, M. M. Frank, M. Tsoi, S. Zollner, V. Narayanan, A.A. Demkov, J. Appl. Phys. 116 (2014) 043705
- [17] K.-H. Kim, H.-S. Kim, M.J. Han, J. Phys. Condens. Matter 26 (2014) 185501.
- Y. Hotta, T. Susaki, H.Y. Hwang, Phys. Rev. Lett. 99 (2007) 236805. T181
- [19] B. Kalisky, E.M. Spanton, H. Noad, J.R. Kirtley, K.C. Nowack, C. Bell, H.K. Sato, M. Hosoda, Y. Xie, Y. Hikita, C. Woltmann, G. Pfanzelt, R. Jany, C. Richter, H. Y. Hwang, J. Mannhart, K.A. Moler, Nat. Mater. 12 (2013) 1091.
- Z. Erlich, Y. Frenkel, J. Drori, Y. Shperber, C. Bell, H.K. Sato, M. Hosoda, Y. Xie, Y. Hikita, H.Y. Hwang, B. Kalisky, J. Supercond. Nov. Magn. 28 (2015) 1017.
- [21] L. Bjaalie, B. Himmetoglu, L. Weston, A. Janotti, C.G. Van de Walle, New J. Phys. 16 (2014) 025005.
- [22] G. Drera, G. Salvinelli, F. Bondino, E. Magnano, M. Huijben, A. Brinkman, L. Sangaletti, Phys. Rev. B 90 (2014) 035124.
- [23] G. Salvinelli, G. Drera, A. Giampietr, L. Sangaletti, ACS Appl. Mater. Interfaces 7 (2015) 25648.
- [24] S. Das, A. Rastogi, L. Wu, Jin-C Zheng, Z. Hossain, Y. Zhu, R.C. Budhani, Phys. Rev. B 90 (2014) 081107(R).
- W. Dai, S. Adhikari, A. Camilo Garcia-Castro, A.H. Romero, H. Lee, J.-W. Lee, S. Eom, C.-B. Ryu, C. Cen, Nano Lett. 16 (2016) 2739.
- [26] D.H. Kim, C.W. Bark, J. Korean Phys. Soc. 68 (2016) 1395.
- S. Adhikari, A.C. Garcia-Castro, A.H. Romero, H. Lee, J.-W. Lee, S. Ryu, C.-B. Eom, [27] C. Cen, Adv. Funct. Mater. 26 (2016) 5453.
- Y. Frenkel, N. Haham, Y. Shperber, C. Bell, Y. Xie, Z. Chen, Y. Hikita, H.Y. Hwang, B. Kalisky, ACS Appl. Mater. Interfaces 8 (2016) 12514.
- [29] C. Cancellieri, A.S. Mishchenko, U. Aschauer, A. Filippetti, C. Faber, O.S. Barisic, V. A. Rogalev, T. Schmitt, N. Nagaosa, V.N. Strocov, Natur Comm. 7 (2016) 10386.
- V.A. Stephanovich, V.K. Dugaev, Phys. Rev. B 93 (2016) 045302.
- [31] S. Das, Z. Hossain, R.C. Budhani, Phys. Rev. B 94 (2016) 115165.
- [32] M. Huijben, G. Rijnders, D.H.A. Blank, S. Bals, S.V. Aert, J. Verbeeck, G. V. Tendeloo, A. Brinkman, H. Hilgenkamp, Nat. Mater. 5 (2006) 556.
- S. Thiel, G. Hammerl, A. Schmehl, C.W. Schneider, J. Mannhart, Science 2006 (1942) 313.
- [34] G. Herranz, M. Basletic, M. Bibes, C. Carretero, E. Tafra, E. Jacquet, K. Bouzehouane, C. Deranlot, A. Hamzic, J.-M. Broto, A. Barthelemy, A. Fert, Phys. Rev. Lett. 98 (2007) 216803.
- M. Balestic, J.-L. Maurice, C. Carretero, G. Herranz, O. Copie, M. Bibes, E. Jacquet, K. Bouzehouane, S. Fusil, A. Barthelemy, Nat. Mater. 7 (2008) 621.

[36] K. Yoshimatsu, R. Yasuhara, H. Kumigashira, M. Oshima, Phys. Rev. Lett. 101 (2008) 026802.

- M. Sing, G. Berner, K. Goss, A. Muller, A. Ruff, A. Wetscherek, S. Thiel, J. Mannhart, S.A. Pauli, C.W. Schneider, P.R. Willmott, M. Gorgoi, F. Schafers, R. Claessen, Phys. Rev. Lett. 102 (2009) 176805.
- [38] R. Pentcheva, W.E. Pickett, Phys. Rev. B 74 (2006) 035112.
- [39] M.S. Park, S.H. Rhim, A.J. Freeman, Phys. Rev. B 74 (2006) 205416.
- [40] S. Ishibashi, K. Terakura, J. Phys. Soc. Jpn. 77 (2008) 104706.
- [41] N. Reyren, S. Thiel, A.D. Caviglia, L.F. Kourkoutis, G. Hammer, C. Richter, C. W. Schneider, T. Kopp, A.-S. Ruetschi, D. Jaccard, M. Gabay, D.A. Muller, J.-M. Triscone, J. Mannhart, Science 317 (2007) 1196.
- [42] A. Brinkman, M. Huijben, M. van Zalk, J. Huijben, U. Zeitler, J.C. Maan, W.G. van der Wiel, G. Rijnders, D.H.A. Blank, H. Hilgenkamp, Nat. Mater. 6 (2007) 493.
- [43] S. Lerer, M.B. Shalom, G. Deutscher, Y. Dagan, Phys. Rev. B 84 (2011) 075423.
- [44] I. Pallecchi, M. Codda, E. Galleani d'Agliano, D. Marre, A.D. Caviglia, N. Reyren, S. Gariglio, J.-M. Triscone, Phys. Rev. B 81 (2010) 085414.
- [45] A. Filippetti, P. Delugas, M.J. Verstraete, I. Pallecchi, A. Gadaleta, D. Marre, D. F. Li, S. Gariglio, V. Fiorentini, Phys. Rev. B 86 (2012) 195301.
- [46] P. Delugas, A. Filippetti, V. Fiorentini, D.I. Bilc, D. Fontaine, P. Ghosez, Phys. Rev. Lett. 106 (2011) 166807.
- [47] Z. Zhong, A. Toth, K. Held, Phys. Rev. B 87 (2013) 161102(R).
- [48] Z. Zhong, P. Wissgott, K. Held, G. Sangiovanni, EPL 99 (2012) 37011.
- [49] R. Arras, V.G. Ruiz, W.E. Pickett, R. Pentcheva, Phys. Rev. B 85 (2012) 125404.
- [50] Z.S. Popovic, S. Satpathy, R.M. Martin, Phys. Rev. Lett. 101 (2008) 256801.
- [51] N. Pavlenko, T. Kopp, E.Y. Tsymbal, G.A. Sawatzky, J. Phys. Rev. B 85 (2012) 020407(R)
- [52] M. Salluzzo, S. Gariglio, D. Stornaiuolo, V. Sessi, S. Rusponi, C. Piamonteze, G. M. De Luca, M. Minola, D. Marre, A. Gadaleta, H. Brune, F. Nolting, N.B. Brookes, G. Ghiringhelli, Phys. Rev. Lett. 111 (2013) 087204.
- [53] A.H. Reshak, M.S. Abu-Jafar, Y. Al-Douri, J. Appl. Phys. 119 (2016) 245303.
- [54] A.H. Reshak, RSC Adv. 6 (2016) 92887.
- [55] T. Fix, J.L. MacManus-Driscoll, M.G. Blamire, Appl. Phys. Lett. 94 (2009) 172101.
- [56] S. Gariglio, M. Gabay, J.-M. Triscone, APL Mater. 4 (2016) 060701.
- [57] J.A. Sulpizio, S. Ilani, P. Irvin, J. Levy, Annu. Rev. Mater. Res. 44 (2014) 117.
- [58] Y.-Y. Pai, A. Tylan-Tyler, P. Irvin, J. Levy, Rep. Prog. Phys. 81 (2018) 036503. [59] Z. Huang, X. Renshaw Ariando, A. Wang, J. Rusydi, H. Chen, T. Venkatesan Yang,
- Adv. Mater. 30 (2018) 1802439. [60] D.V. Christensen, F. Trier, W. Niu, Y. Gan, Y. Zhang, T.S. Jespersen, Y. Chen, N. Pryds, Adv. Mater. Interfaces 6 (2019) 1900772.
- [61] L. Kornblum, Adv. Mater. Interfaces 6 (2019) 1900480.
- [62] J.P. Perdew, S. Burke, M. Ernzerhof, Phys. Rev. Lett. 77 (1996) 3865.
- [63] E. Engel, S.H. Vosko, Phys. Rev. B 47 (1993) 13164.
- [64] V.I. Anisimov, F. Aryasetiawan, A.I. Liechtenstein, J. Phys. Condens. Matter 9 (1997) 767.
- [65] J. Lee, A. Demkov, Phys. Rev. B 78 (2008) 193104.
- [66] R. Pentcheva, W.E. Picket, Phys. Rev. B 78 (2008) 205106.
- [67] Z. Zhong, P.J. Kelly, Europhys. Lett. 84 (2008) 27001.
- [68] P. Dufek, P. Blaha, K. Schwarz, Phys. Rev. B 50 (1994) 7279. [69] A. Mokhtari, H. Akbarzadeh, Physica B 337 (2003) 122.
- [70] P. Blaha, K. Schwarz, G.K.H. Madsen, D. Kvanicka, J. Luitz, WIEN2K, an Augmented Plane Wave + Local Orbital Program forCalculating Crystal Properties Karlheinz Schwarz; Techn, Universitat, Wien, Austria, 2001. ISBN: 3-9501031-1-
- [71] A.H. Reshak, S. Auluck, I.V. Kityk, J. Phys. Condens. Matter 20 (2008) 145209.
- [72] A.H. Reshak, S. Auluck, I.V. Kityk, J. Solid State Chem. 181 (2008) 789-795.
- [73] A.H. Reshak, I.V. Kityk, S. Auluck, J. Phys. Chem. B 114 (2010) 16705–16712.
- [74] A.H. Reshak, S. Auluck, D. Stys, I.V. Kityk, H. Kamarudin, J. Berdowski, Z. Tylczynskif, J. Mater. Chem. 21 (2011) 17219.
- [75] A.H. Reshak, M. Piasecki, S. Auluck, I.V. Kityk, R. Khenata, B. Andriyevsky, C. Cobet, N. Esser, A. Majchrowski, M. S'wirkowicz, R. Diduszko, W. Szyrski, J. Phys. Chem. B 113 (46) (2009) 15237.
- [76] B.F. Ding, H.J. Qian, C. Han, J.Y. Zhang, S.E. Lindquist, B. Wei, Z.L. Tang, J. Phys. Chem. C 118 (2014) 25633.
- [77] J. Kübler, A.R. Williams, C.B. Sommers, Phys. Rev. B 28 (1983) 1745.
- [78] S. Sharma, S.K. Pandey, J. Phys. Condens. Matter 26 (2014) 215501.
- [79] S. Ouardi, B. Balke, A. Gloskovskii, G.H. Fecher, C. Felser, G. Schönhense, T. Ishikawa, T. Uemura, M. Yamamoto, H. Sukegawa, W. Wang, K. Inomata, Y. Yamashita, H. Yoshikawa, S. Ueda, K. Kobayashi, J. Phys. D, Appl. Phys. 42 (2009) 084010.
- [80] W. Wunderlich, H. Ohta, K. Koumoto, Physica B 404 (2009) 2202.
- [81] Q.L. Chen, B. Li, G. Zheng, K.H. He, A.S. Zheng, Physica B 406 (2011) 3841.
- [82] C. Lin, D. Shin, A. Demkov, J. Appl. Phys. 117 (2015) 225703.
- [83] G. Khalsa, A.H. MacDonald, Phys. Rev. B 86 (2012) 125121.
- [84] A.H. Reshak, S. Azam, J. Magn. Magn. Mater. 342 (2013) 80.